Comparative genomic analysis of clinical *Candida glabrata* isolates identifies multiple polymorphic loci that can improve existing multilocus sequence typing strategy

A. Arastehfar[1,9], M. Marcet-Houben[3,4,5,9], F. Daneshnia[1], S.J. Taj-Aldeen[6], D. Batra[7], S.R. Lockhart[7], E. Shor[1,2*], T. Gabaldón[3,4,5*], and D.S. Perlin[1,2,8]

[1]Center for Discovery and Innovation, Hackensack Meridian Health, Nutley, NJ, 07110, USA; [2]Hackensack Meridian Health School of Medicine, Nutley, NJ, 07710, USA; [3]Barcelona Supercomputing Centre (BSC-CNS), Jordi Girona 29, 08034, Barcelona, Spain; [4]Institute for Research in Biomedicine (IRB Barcelona), The Barcelona Institute of Science and Technology, Baldiri Reixac 10, 08028, Barcelona, Spain; [5]Catalan Institution for Research and Advanced Studies (ICREA), Barcelona, Spain; [6]Hamad Medical Corporation, Doha, Qatar; [7]Mycotic Diseases Branch, Centers for Disease Control and Prevention, Atlanta, GA, 30329, USA; [8]Georgetown University Lombardi Comprehensive Cancer Center, Department of Microbiology and Immunology, Washington, DC, 20057, USA

*Correspondence: E. Shor, erika.shor@hmh-cdi.org; T. Gabaldón, toni.gabaldon.bcn@gmail.com
[9]AA and MMH equally contributed to this work.

Abstract: *Candida glabrata* is the second leading cause of candidemia in many countries and is one of the most concerning yeast species of nosocomial importance due to its increasing rate of antifungal drug resistance and emerging multidrug-resistant isolates. Application of multilocus sequence typing (MLST) to clinical *C. glabrata* isolates revealed an association of certain sequence types (STs) with drug resistance and mortality. The current *C. glabrata* MLST scheme is based on single nucleotide polymorphisms (SNPs) at six loci and is therefore relatively laborious and costly. Furthermore, only a few high-quality *C. glabrata* reference genomes are available, limiting rapid analysis of clinical isolates by whole genome sequencing. In this study we provide long-read based assemblies for seven additional clinical strains belonging to three different STs and use this information to simplify the *C. glabrata* MLST scheme. Specifically, a comparison of these genomes identified highly polymorphic loci (HPL) defined by frequent insertions and deletions (indels), two of which proved to be highly resolutive for ST. When challenged with 53 additional isolates, a combination of *TRP1* (a component of the current MLST scheme) with either of the two HPL fully recapitulated ST identification. Therefore, our comparative genomic analysis identified a new typing approach combining SNPs and indels and based on only two loci, thus significantly simplifying ST identification in *C. glabrata*. Because typing tools are instrumental in addressing numerous clinical and biological questions, our new MLST scheme can be used for high throughput typing of *C. glabrata* in clinical and research settings.

Key words: *Candida glabrata*, MLST, Sequence type, Whole-genome sequencing.

INTRODUCTION

Candida species are among the most prevalent mycobiome constituents (Romo & Kumamoto 2020) and also a major cause of invasive fungal infections in humans worldwide (Brown *et al.* 2012). It has been estimated that > 400 000 life-threatening infections are caused by *Candida albicans* alone (Brown *et al.* 2012). Although *C. albicans* once was the most prevalent cause of candidemia, recent studies have revealed a stark increase in candidemias caused by non-*albicans Candida* (NAC) species, especially *C. glabrata*, *C. parapsilosis*, and *C. tropicalis* (Astvad *et al.* 2018, Lamoth et al., 2018, Fuller *et al.* 2019; Pfaller et al., 2019, Song *et al.* 2020, Stavrou et al., 2019; Won *et al.* 2021). *Candida glabrata* has been identified as the second leading cause of candidemia in the US (Pfaller *et al.* 2009, Pfaller et al., 2019, Tsay *et al.* 2020), Canada (Fuller *et al.* 2019), Australia (Chapman *et al.* 2017), and some European (Astvad *et al.* 2018) and Asian countries (Taj-Aldeen *et al.* 2014, Arastehfar *et al.* 2020a, Kord *et al.* 2020). *Candida glabrata* has reduced susceptibility to fluconazole (Healey & Perlin 2018, Arastehfar *et al.* 2020b) and can rapidly develop drug resistance during infection (Healey & Perlin 2018, Ksiezopolska & Gabaldón 2018, Arastehfar *et al.* 2020b). Indeed, the increasing incidence of

candidemia due to *C. glabrata* in recent years has coincided with a notable increase in the number of fluconazole-resistant (FLZR) isolates in many countries (Hou *et al.* 2017, Astvad *et al.* 2018, Pfaller et al., 2019, Arastehfar *et al.* 2020c, Won *et al.* 2021). Patients infected with FLZR *C. glabrata* isolates had the highest mortality rate and experienced a shorter median survival days after diagnosis compared to those infected with fluconazole-susceptible-dose-dependent (FLZ-SDD) isolates (Won *et al.* 2021). These observations are especially concerning for developing countries, where fluconazole is the frontline antifungal drug used to treat candidemia (Chakrabarti *et al.* 2015, Arastehfar *et al.* 2020d, Kord *et al.* 2020, Megri *et al.* 2020). However, the emerging echinocandin-resistant (ECR) and multidrug-resistant (MDR) *C. glabrata* isolates, which constitute > 30 % of the ECR isolates (Astvad *et al.* 2018, Won *et al.* 2021), may also threaten the clinical efficacy of echinocandins, the frontline antifungal drugs recommended by international guidelines (Pappas et al., 2016). Together, these features make *C. glabrata* one of the most challenging fungal pathogens of the present time.

Although *C. glabrata* is considered to be predominantly asexual, various types of genome analyses of *C. glabrata* clinical isolates revealed a high degree of genetic diversity both in terms

of chromosome structure and sequence (Carreté *et al.* 2018, Xu *et al.* 2021), and this diversity was estimated to be greater than that of *C. albicans* (Carreté *et al.* 2018, Gabaldón & Fairhead 2019). Understanding the genetic diversity of *C. glabrata* isolates from both clinical and biological standpoints is of paramount importance, as it will help to answer key questions regarding its epidemiology, aid in implementing appropriate infection control strategies by identifying the route of infection (Megri *et al.* 2020), and also enables researchers to uncover the evolution of drug resistance of genetically-related isolates during the course of infection (Carreté *et al.* 2019). Additionally, several studies have uncovered an association between genotype and mortality (Byun *et al.* 2018, Arastehfar *et al.* 2019) and drug resistance (Won *et al.* 2021). Studies dissecting the genetic structure of *C. glabrata* isolates have employed various tools, such as whole-genome sequencing (WGS) (Biswas *et al.* 2018, Carreté *et al.* 2018, 2019), polymorphic locus sequence typing (Katiyar *et al.* 2016, Katiyar & Edlind 2021), pulsed field gel electrophoresis (PFGE) (Lin *et al.* 2007), amplified fragment length polymorphism analysis (Arastehfar *et al.* 2019), multilocus microsatellite typing (MLMT) (Hou et al., 2018, Bordallo-Cardona et al., 2019, Arastehfar *et al.* 2020c), and multilocus sequence typing (MLST) (Lott *et al.* 2010, 2012, Hou *et al.* 2017, Hou et al., 2018, Byun *et al.* 2018, Bordallo-Cardona et al., 2019, Khalifa *et al.* 2020, Won *et al.* 2021). Among these, WGS provides the most information and resolution, and short read based and nanopore long read based sequencing platforms are gradually becoming more accessible and affordable (Gabaldón 2019). However, the extensive chromosome structure diversity between clinical isolates makes it difficult to use standard tools for short read sequence analysis, which rely on mapping the reads to a reference genome with a common structure. Therefore, there is a need for additional high quality assembled *C. glabrata* genomes that can serve as references, facilitating WGS analysis of clinical isolates.

Although WGS provides the most information and resolution, the still high costs and sophisticated analysis hinder its wide use in clinical settings, especially among medical mycologists (Gabaldón *et al.* 2020). Therefore, most of the studies conducted so far have used MLMT and MLST as the most popular techniques to type clinical *C. glabrata* isolates (Gabaldón *et al.* 2020). The MLST method is highly reproducible and provides data that are consistent with WGS (Carreté *et al.* 2018). These data can be archived at "https://pubmlst.org/organisms/candida-glabrata" (Gabaldón *et al.* 2020), making the worldwide, temporal, and nationwide analysis of clinical *C. glabrata* isolates possible. The currently used MLST scheme (Dodgson *et al.* 2003) has identified 1 414 isolates of *C. glabrata* belonging to > 100 STs, which underscores its genetic diversity. This scheme is based on SNPs at six loci (*FKS1*, *LEU2*, *NMT1*, *TRP1*, *UGP1*, and *URA3*), together comprising > 3 000 bps. Of course, it is desirable to reduce the required number of loci to reduce the time and cost associated with MLST analysis, without losing resolutive power.

In this study, we obtained high quality genome data based on PacBio and Illumina sequencing for seven additional clinical isolates of *C. glabrata* belonging to ST10, 15, and 16. Comparative analysis of the seven genomes identified a number of highly polymorphic loci (HPL) characterized by a high number of insertions/deletions (indels). These loci were enriched for the functional categories governing stress response pathways, particularly those involved in membrane and cell wall stresses. Interestingly, we found that two of these HPLs were highly resolutive for ST identity. Using an additional set of 53 clinical

isolates showed that each of these loci in combination with *TRP1* provided the same resolution as that generated by the traditional six-locus MLST protocol (Dodgson *et al.* 2003). Therefore, we propose an improved MLST protocol for *C. glabrata*, which necessitates sequencing only two loci (totalling ≤1 Kbp) and offers a quicker and cheaper approach without the loss of resolution, and which can be used for high throughput typing studies of *C. glabrata*.

MATERIALS AND METHODS

Isolates and growth conditions

The 53 *C. glabrata* strains used in this study are listed in Table 1. The isolates originated from various geographical regions and had various antifungal susceptibility profiles. All isolates were grown on yeast peptone dextrose (YPD) agar and incubated at 37 °C for 24–48 h.

To enrich the genomes available for comparative purposes and due to the limited number of high-quality genome data, we performed whole-genome PacBio and Illumina sequencing of seven isolates, DPK305, CAS08-0425, DPK762, DPL1021, CAS080027, DPL245, CAS08-0016 (Table 1), which belonged to three STs (10, 15, and 16) and had different susceptibility profiles.

Antifungal susceptibility testing (AFST)

Antifungal susceptibility testing (AFST) followed the CLSI-M60 (Clinical and Laboratory Standards Institute. 2017) protocol and included fluconazole (Pfizer, New York, NY, USA), amphotericin B (AMB) (Sigma-Aldrich, Milwaukee, WI, USA), micafungin (Astellas Pharma, Tokyo, Japan), and anidulafungin (Pfizer). Plates containing antifungal drug-*C. glabrata* cell suspensions were incubated at 37 °C for 24 h and minimum inhibitory concentrations (MICs) were visually recorded. Type strains of *C. krusei* (ATCC 6258) and *C. parapsilosis* (ATCC 22019) were used in each individual AFST experiment for quality control purposes. Susceptibility profiles were denoted based on the availability of the clinical breakpoints and epidemiological cutoff values (ECVs) as suggested (Pfaller & Diekema 2012). Briefly, isolates showing MIC ≥ 64 µg/ml, ≥ 0.5 µg/ml, and ≥ 0.25 µg/ml were regarded as fluconazole-resistant, anidulafungin-resistant, and micafungin-resistant, respectively (Pfaller & Diekema 2012). The MIC data of AMB was interpreted based on ECVs and isolates showing a MIC > 2µg/ml were regarded as non-wild-type (Pfaller & Diekema 2012).

DNA extraction

The DNA extraction method varied depending on the sequencing method used. DNA samples subjected to Illumina and Sanger sequencing were extracted using the Quick-DNA Fungal/Bacterial Miniprep Kit (ZymoResearch, Irvine, CA, USA) following the protocol suggested by manufacturer. DNA isolation for PacBio sequencing followed an old-fashioned DNA isolation protocol. Briefly, overnight *C. glabrata* cultures were harvested by centrifugation, the cells were disrupted by vortexing in lysis buffer (100 mM Tris pH 8.0; 50 mM EDTA; 1 % SDS), and the liquid phase was collected. This was followed by incubation with

Table 1. List of clinical *Candida glabrata* isolates used in this study.

Isolate #	Original #	Sequence type	Minimum inhibitory concentration (µg/ml)				Susceptibility profiles	Comments
			Fluconazole	Micafungin	Anidulafungin	AMB		
1	CAS08-0293	ST3	64	4	4	1	MDR	
2	CAS08-0725 (CMD00311)	ST3	64	0.5	2	1	MDR	
3	CAS09-0869 (CMD00373)	ST3	64	0.5	2	1	MDR	
4	BG2	ST3	4	0.015	0.125	1	S	
5	Qatar 36	ST3	4	0.015	0.125	0.5	S	
6	DPK 159	ST3	4	0.015	0.125	1	S	
7	DPL27 (5962)	ST3	4	2	4 or 2	1	ECR	
8	ATCC 66032	ST6	4	0.015	0.06	0.5	S	
9	CAS09-1225 (CGA00908)	ST6	> 64	4	2	2	MDR	
10	CAS09-1786 (CGA01258)	ST6	64	4	2	1	MDR	
11	DPL155 (M234)	ST6	1	0.25	1	1	ECR	
12	DPL157 (17351, CGC2)	ST6	64	4	4	1	MDR	
16	CAS08-0089	ST8	4	0.015	0.125	1	S	
17	CAS08-494	ST8	4	0.015	0.125	1	S	
18	CAS08-528	ST8	4	0.015	0.125	1	S	
19	CAS11-3112 (CGA02083)	ST8	64	0.25	0.5	1	MDR	
20	DPL209 (M2952)	STX	64	4	4	1	MDR	
25	CAS08-0205	ST10	4	0.015	0.125	0.5	S	
26	CAS09-1083 (CGA00822)	ST10	64	0.5	1	0.5	MDR	
27	CAS09-1437 (CGA01045)	ST10	64	2	1 or 0.5	1	MDR	
28	DPK 305	ST10	4	0.015	0.125	1	S	WGS
29	CAS08-0425 (CMD00008)	ST10	64	4	4	1	MDR	WGS
35	DPL1021 (ATCC 90030)	ST10	4	0.015	0.125	1	S	WGS
21	Qatar 38	ST15	4	0.015	0.25	1	S	
22	Qatar 57	ST15	4	0.015	0.125	1	S	
23	Qatar 71	ST15	> 64	0.06	0.25	1	FLZR	
24	ATCC 2001 (CBS 138)	ST15	4	0.015	0.125	0.5	S	
30	CAS08-0027	ST15	64	0.015	0.125	1	FLZR	WGS
31	CAS08-485	ST15	4	0.015	0.125	1	S	
32	CAS09-755	ST15	4	0.015	0.125	1	S	
33	DPK 762	ST15	4	0.015	0.125	1	S	WGS
34	DPL274 (3-CPH-W20800)	ST15	1	1	4	4	ECR	
36	CAS08-0092	STY	2	0.015	0.125	1	S	
37	CAS11-3129 (CMD01408	STY	64	4	4	0.5	MDR	
38	DPL245 (1611)	STY	16	4	4	0.5	ECR	WGS
39	DPL38 (42997)	STY	32	1	2	0.25	ECR	
40	CAS08-0016 (CGA00019)	STY	64	2	1	1	MDR	WGS
41	DPL217	ST17	2	0.5	1	0.5	ECR	
42	DPL219	ST17	2	0.5	1	0.5	ECR	
44	LB599-02	ST46	4	0.015	0.125	1	S	

(continued on next page)

Table 1. (Continued).

Isolate #	Original #	Sequence type	Minimum inhibitory concentration (µg/ml)				Susceptibility profiles	Comments
			Fluconazole	Micafungin	Anidulafungin	AMB		
45	LB906-05	ST46	64	0.015	0.125	1	FLZR	
46	Qatar 51	ST46	2	0.015	0.125	1	S	
48	Qatar 59	ST46	2	0.015	0.06	1	S	
50	Qatar 62	ST46	2	0.015	0.06	1	S	
53	Qatar 69	ST46	4	0.03	0.25	1	S	
54	Qatar 72	ST46	64	0.015	0.125	1	FLZR	
56	Qatar 76	ST46	4	0.015	0.125	1	S	
47	Qatar 53	ST7	2	0.015	0.06	1	S	
49	Qatar 61	ST7	4	0.015	0.06	1	S	
51	Qatar 63	ST7	4	0.015	0.06	1	S	
52	Qatar 64	ST7	2	0.015	0.06	1	S	
55	Qatar 73	ST7	4	0.015	0.125	1	S	
57	CAS08-0094	ST76	> 64	2	4	1	MDR	

AMB: Amphotericin B, MDR: Multidrug-resistant, S: Susceptible, ECR: Echinocandin-resistant, FLZR: Fluconazole-resistant, WGS: Whole-genome sequenced.

ammonium sulphate, followed by chloroform extraction, and isopropanol precipitation. Finally, the pellets were washed with 70 % ethanol, air-dried, and resuspended in RNase/DNase free water.

Illumina library preparation and WGS

Genomic DNA was quantified using the Qubit v. 2.0 Fluorometer (Life Technologies, Carlsbad, CA, USA). The DNA integrity was checked with ~1 % agarose gel with 50–100 ng sample loaded in each well. Samples were then chosen for library preparation based on the QC results. NEBNext® Ultra™ II DNA Library Prep Kit for Illumina, clustering, and sequencing reagents were used throughout the process following the manufacturer's recommendations. Briefly, the genomic DNA was fragmented by acoustic shearing with a Covaris S220 instrument. Fragmented DNA was cleaned up and end repaired. Adapters were ligated after adenylation of the 3' ends followed by enrichment by limited cycle PCR. DNA libraries were validated using a DNA 1000 Chip on the Agilent 2100 Bioanalyzer (Agilent Technologies, Palo Alto, CA, USA), and were quantified using Qubit v. 2.0 Fluorometer. The DNA libraries were also quantified by real-time PCR (Applied Biosystems, Carlsbad, CA, USA), clustered on one lane of a flowcell, and loaded on the Illumina HiSeq instrument according to manufacturer's instructions. The samples were sequenced using a 2× 150 paired-end (PE) configuration. Image analysis and base calling were conducted by the HiSeq Control Software (HCS) on the HiSeq instrument. Raw sequence data (.bcl files) generated from Illumina HiSeq were converted into fastq files and demultiplexed using Illumina's bcl2fastq v. 2.17 software. One mismatch was allowed for index sequence identification.

PacBio library preparation and genome assembly

PacBio DNA sequencing of *C. glabrata* strains was performed at the Waksman Institute, Rutgers University. Library preparation closely followed the multiplexed microbial library

protocol provided by Pacific Biosciences. Briefly, the DNA quality was evaluated using a Qubit fluorometer (Thermo Fisher Scientific, Waltham, MA, USA) and Nanodrop spectrophotometer (Thermo Fisher Scientific). Two micrograms genomic DNA was fragmented using Magaruptor (Diagenode, Glen Ridge, NJ, USA) with the 10 kbp fragments settings according to the manufacturer's instructions. This is followed by 0.45× AMPure PB Bead Purification and removal of Single-Strand Overhangs. Samples were then subjected to DNA Damage Repair, End Repair, A-tailing and ligation to prepare SMRTbell DNA template libraries. After another round of 0.45× PB Bead Purification libraries were pooled in equimolar ratio and size selected with BluePippin (Sage Science, Beverly, MA, USA). Library quality was analysed by Qubit, and average fragment size was estimated using an Agilent Fragment Analyzer (Agilent, Santa Clara, CA, USA). SMRT sequencing was performed using a Pacific Biosciences Sequel I sequencer (PacBio, Menlo Park, CA, USA) and standard protocols (MagBead Standard Seq v. 2 loading, 600 min movie) using SMRT Cell 1M v. 2. Single molecule real-time sequencing reads were demultiplexed using SMRT Analysis software suite v. 5.1 (Pacific Biosciences Inc., Menlo Park, CA, USA) and *de novo* assembled using the CANU v. 1.7 workflow (Koren *et al.* 2017). Scaffolding was performed using the SSPACE long-read scaffolder (Boetzer & Pirovano 2014). Genome assembly was further improved for assembly contiguity using PBJelly (English *et al.* 2012). The PBJelly running parameters were as follows: -minMatch 8 -sdpTupleSize 8 -minPctIdentity 75 -bestn 1 -nCandidates 10 -maxScore -500 -nproc 13 -noSplitSubreads. WGS data obtained from Illumina was used to correct the those generated by PacBio. SNP calling was performed by aligning reads from each strain to each of the other strains using BWA mem v. 0.7.17-r1188 (Li & Durbin 2009) and GATK v. 4.0.4.0 (DePristo *et al.* 2011).

Annotation and gene prediction

Gene prediction was performed using a combination of methods. Reference sets were formed by the annotation of the

reference genome of *C. glabrata*, and the collection of proteomes used in YGOB (Byrne & Wolfe 2005). Exonerate v. 2.4.0 (Slater & Birney 2005) was used to search for the presence of each protein in YGOB against each of the genomes. RATT (Otto *et al.* 2011) (downloaded 2018) from the PAGIT package was used to transfer annotations from the *C. glabrata* reference genome to the strain genomes; it was run in three modes: strain, species and multi, and the best transference was kept. YGAP web server (Proux-Wéra *et al.* 2012) (accessed October 2020) was then used to obtain a second gene prediction. MAKER2 v. 2.31.10 (Holt & Yandell 2011) was the third annotation program used. Results from RATT, YGAP, MAKER and exonerate were joined together into a single gene prediction using EVM (Haas *et al.* 2008) (downloaded 2018). This annotation was then improved by searching for the presence of genes that were predicted in the *C. glabrata* reference but not included in the strain annotation. As *C. glabrata* strains tend to be highly syntenic, the pipeline first associated each predicted protein in the strain genome to the reference genome using a best reciprocal hit approach. Then, based on location, it tried to associate unmatched genes if enough similarity was found even if they were not best reciprocal hits. In the same way it corrected spurious matches that were not congruent with the gene order conservation. Once the list of missing genes was found, the pipeline scanned the RATT annotation for those genes. If found they were incorporated to the gene prediction, if not the pipeline located surrounding genes and then used GenomeThreader v. 1.7.1 (Gremme *et al.* 2005) to search the intergenic space between those genes for the presence of the missing genes. In a last step, for genes still not found, the whole genome was scanned for their presence.

Identification of highly polymorphic loci (HPL) and primer design

Individual chromosomes of the seven clinical isolates (Table 1) were aligned with those of the reference strain CBS138/ ATCC2001 (Xu *et al.* 2021) and strain DSY562 (Vale-Silva *et al.* 2017) using the Mauve alignment tool (DNASTAR, Madison, USA). Highly polymorphic loci (HPL) were defined based on the presence of indels that were different between strains of different STs. To avoid overlap with previously published sets of loci, HPL associated with satellite regions, megasatellites, minisatellites, and microsatellites, were excluded (Thierry *et al.* 2008). Loci obtained were subjected to gene ontology (GO) enrichment using FungiFun (Priebe *et al.* 2015), and those involved in cellular integrity pathways (osmotic stress tolerance, cell wall integrity and membrane integrity pathways, *etc.*) were selected for primer design. The primers were chosen to amplify the shortest possible regions without losing any indel information. All primer information is listed in Table 2.

MLST schemes used and tree construction

The original MLST scheme developed by Dodgson *et al.* (2003) was used as the gold standard (Dodgson *et al.* 2003). Strain types (STs) were determined with the use of the https://pubmlst. org/about-us database. For each strain, a BLAST search was

Table 2. Oligos used in this study, their functions, and their PCR conditions.

Oligo name	Function	Oligo sequence (5'–3')
USA1-F	PCR/Sequencing	CCTGGAGAAGATGTATGTGTT
USA1-R	PCR/Sequencing	TCTTCATGGTCGTGCTGAT
DUF1-F	PCR/Sequencing	TATCAAGTGTGTGGTGCC
DUF1-R	PCR/Sequencing	CGTGTTCGACAGATTGTCC
SLG1-F	PCR/Sequencing	GATGCTACTTATACTGGCGG
SLG1-R	PCR/Sequencing	TCAATCGGTTTCGTCTGG
HKR1-F	PCR/Sequencing	GAGAAAGCTATTGCTTTTGGT
HKR1-R	PCR/Sequencing	TCAATAGATGATGGCTGCAC
H09053-F	PCR/Sequencing	AATACGAAAGCCACGACG
H09053-R	PCR/Sequencing	ATATCTGGAATGCACTACCTG
A02255-F	PCR/Sequencing	TGGATTCGAATGAGGGACT
A02255-R	PCR/Sequencing	CGAGTTCACACCGATTATCC
G00825-Fex	PCR/Sequencing	TCAAATGCTCCTCCTGGC
C00825-F1	Sequencing	CTCTACAGGCGGCAAAA
G00825-R1	Sequencing	GAATAATTAGAGTCGCCTCCG
25F-N	Sequencing	TGG CAG AAA TAA ACG CCA G
G00825-Rex	PCR/Sequencing	CCAACATCAATTTCAGGAGC
SSR1-F	PCR/Sequencing	GAGCTGGAACTCGATCCG
SSR1-R	PCR/Sequencing	AGGAAGGGGAGTAATGATGG
PIR2-F	PCR/Sequencing	ATGCAATACAAAAAGACTCTAGC
PIR2-R	PCR/Sequencing	TGGATCATTTGGTGCCTTAC
PIR1-F	PCR/Sequencing	CTTCTTCCTCTGTCGCTAAG
PIR1-R	PCR/Sequencing	CAATTTGAGAAGCAGCGC
C00715-F	PCR/Sequencing	AGCCTCTGTCCCTACTTTATC
C00715-R	PCR/Sequencing	GTCGCTGTTGGTGTGTAA
G03839-F	PCR/Sequencing	CCCAATCCCTTTCTCTGCT
G03839-R	PCR/Sequencing	TATCCTCTTCTCATCGCTCG
G06281-F	PCR/Sequencing	GATGTTATGGTCTAGCTTTGC
G06281-R	PCR/Sequencing	CTGCCTATCTTAGATTGCTAGA

Note that except for G00825 and PIRI, the rest of the loci had the same PCR program (94 °C 5 mins, 35 cycles of (94 °C 30 s, 60 °C 30 s, 72 °C 40 s), 72 °C 8 mins). PCR programs for G00825 was 94 °C 5 mins, 35 cycles of (94 °C 30 s, 58 °C 30 s, 72 °C 2 mins), 72 °C 8 mins and for PIRI was 94 °C 5 mins, 35 cycles of (94 °C 30 s, 58 °C 30 s, 72 °C 40 s), 72 °C 8 mins.

performed to determine the allele identity of each gene. Then the allelic combination was introduced in order to identify the STs. In one case, the allelic combination did not produce a known sequence type, and was named STX.

The trees obtained from the MLST scheme based on HPL were categorised as follows: trees that were obtained based on the concatenation of all 13 HPL, those constructed based on each individual HPL, those generated based on combination of two most resolutive HPL, and trees constructed based on the combination of the most resolutive HPL in combination with each loci of the original MLST scheme (Dodgson *et al.* 2003).
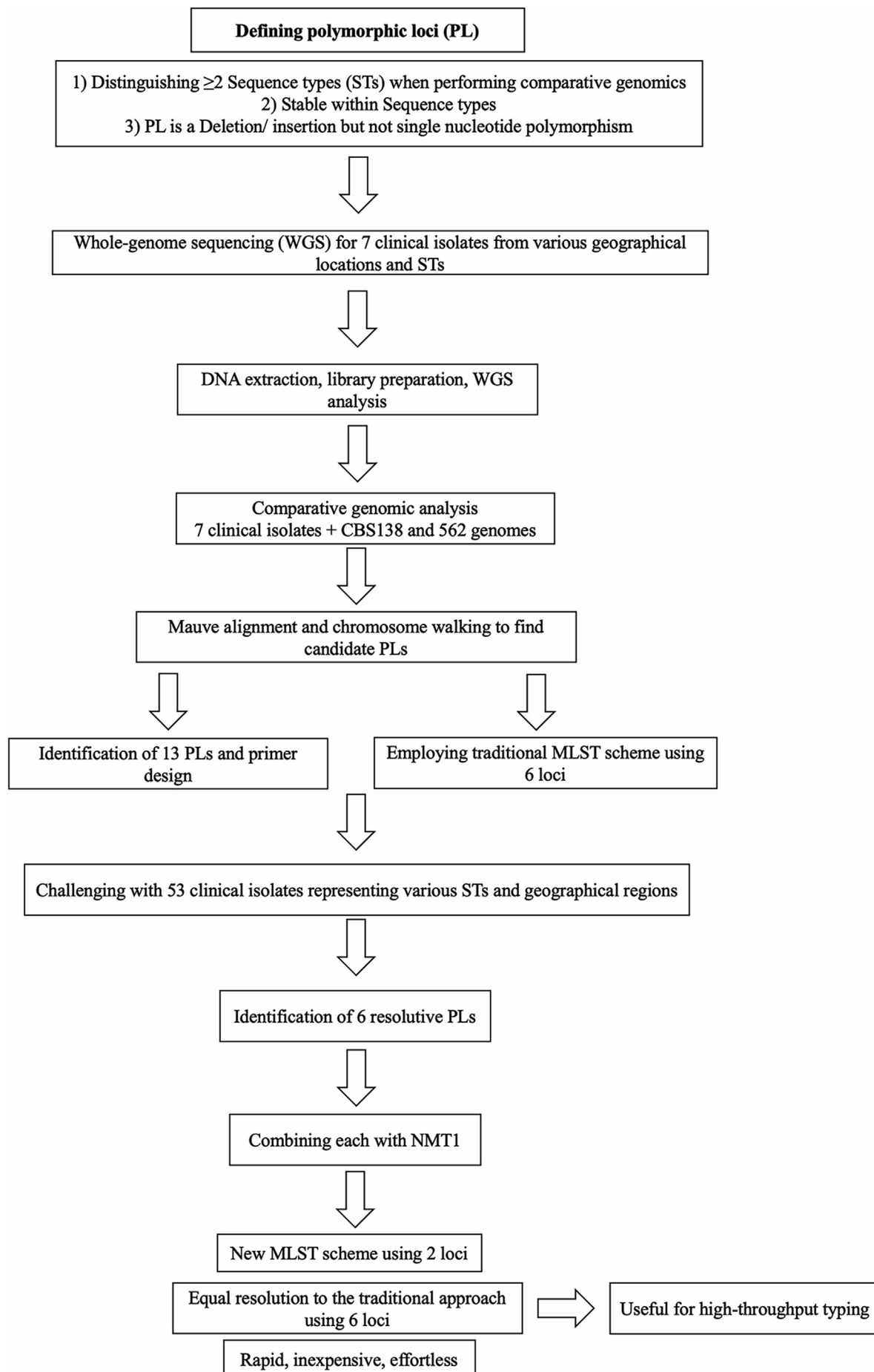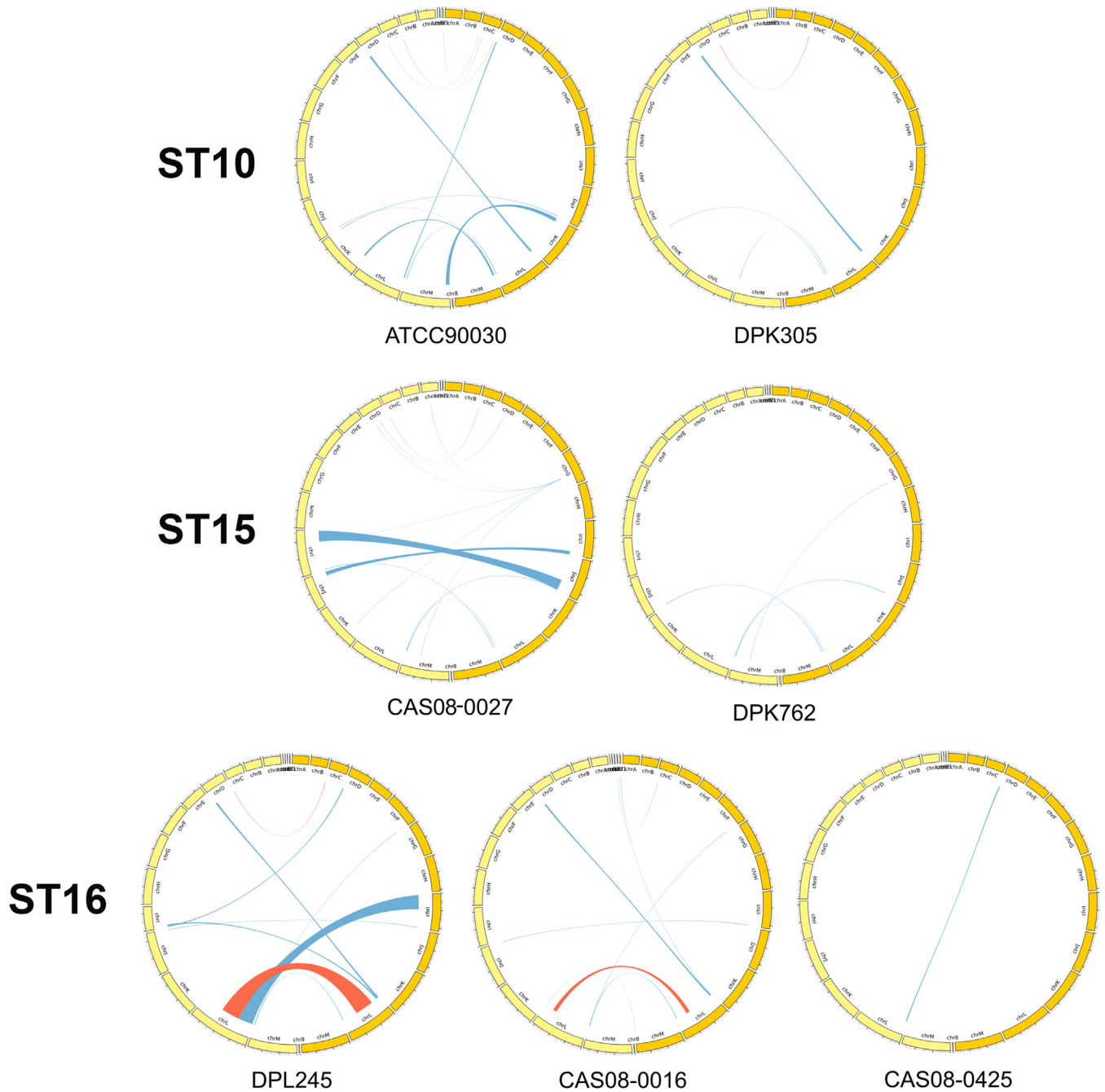
Defining polymorphic loci (PL)

1) Distinguishing ≥2 Sequence types (STs) when performing comparative genomics
2) Stable within Sequence types
3) PL is a Deletion/ insertion but not single nucleotide polymorphism

⇩

Whole-genome sequencing (WGS) for 7 clinical isolates from various geographical locations and STs

⇩

DNA extraction, library preparation, WGS analysis

⇩

Comparative genomic analysis
7 clinical isolates + CBS138 and 562 genomes

⇩

Mauve alignment and chromosome walking to find candidate PLs

⇩   ⇩

Identification of 13 PLs and primer design   Employing traditional MLST scheme using 6 loci

⇩

Challenging with 53 clinical isolates representing various STs and geographical regions

⇩

Identification of 6 resolutive PLs

⇩

Combining each with NMT1

⇩

New MLST scheme using 2 loci

Equal resolution to the traditional approach using 6 loci   ⇨   Useful for high-throughput typing

Rapid, inexpensive, effortless

Fig. 1. The workflow of finding hyperpolymorphic loci (HPL) in this study.

Fig. 2. Circos plots representing inversions (red) and translocations (blue) between the genomes of the *C. glabrata* reference strain (dark yellow on the right of each circle) and each individual strain (light yellow on the left of each circle). Chromosomes are ordered as mirror images of each other, starting with chromosome A at the top and ending with chromosome M at the bottom of the image.

Table 3. Polymorphic loci of interest identified through comparative whole-genome sequencing.

Polymorphic loci	Standard names	Systematic names
CHS5/ CAGL0G00814g	*CHS5*	YLR330W
G00715/ CAGL0G00858g[1]	*IEA* with *MID2*	YLR332W
G00825/ CAGL0G00968g[1]	*VRP1*	YLR337C
SRP40/ CAGL0G02409g	*SRP40*	YKR092C
G03839/ CAGL0G03993g[1]	*N/A*	Not available
G06281/ CAGL0G06446g[1]	*N/A*	Not available
G07117/ CAGL0G07293g[1]	*USA1*	YML029W
SSR1/ CAGL0H06413g[1]	*CCW14*	YLR390W-A
H09053/ CAGL0H09152g[1]	*PTK1*	YKL198C
PIR2/ CAGL0I06182g	*SHP150*	YJL159W
I07645/ CAGL0I07821g[1]	*DUF1*	YOL087C
K01793/ CAGL0K01947g	*YER137C*	YER137C
K06501/ CAGL0K06655g	*NGR1*	YBR212W
K09845/ CAGL0K10010g	*PRP8*	YDR083W
PIR3/ CAGL0M08492g[1]	*PIR1*	YKL164C
M09053/ CAGL0M09086g	*BUD4*	YJR092W
M09075/ CAGL0M09108g	*JSN1*	YJR091C
GVI51_A02255/ CAGL0A02486g[1]	*SEB2*	YDR351W
A00825/ CAGL0A01001g[1]	*YLR326W*	YLR326W
A02431/ CAGL0A02651g	*EAF1*	YDR359C
C01617/ CAGL0C01859g	*RER1*	YCL001W
ARB1/ CAGL0C02343g	*ARB1*	YER036C
C02321/ CAGL0C02541g	*BDF1*	YLR399C
POP2/ CAGL0C03399g	*POP2*	YNR052C
ABP1/ CAGL0C03597g	*ABP1*	YCR088W
D02871/ CAGL0D02926g	*BRE2*	YLR015W
D05049/ CAGL0D05082g	*UBI4*	YLL039C
E00341/ CAGL0E00561g	*TUP1*	YCR084C
SWI5/ CAGL0E01331g	*SWI5*	YDR146C
STP8/ CAGL0F01837g	*SPT8*	YLR055C
SLG1[1]	*SLG1*	YOR008C
HKR1/ CGAL0F03003g[1]	*HKR1*	YDR420W
F03333/ CAGL0F03641g	*YML018C*	YML018C

[1] These were the 13 polymorphic loci that were selected for MLST analysis in this study.

Robinson and Foulds comparison

ETE v. 3 was used to calculate the normalized Robinson and Foulds (RF) distances between trees (Huerta-Cepas *et al.* 2010). To calculate this value trees were first rooted to one of the leaves so that all trees had potentially the same structure. The RF calculates the number of common partitions between two trees. Normalization was carried out by dividing this value over the total number of partitions found in both trees. A high RF indicates little overlap between the two trees, although a single leaf moving to a

Table 4. Statistics for trees based on individual genes. MLST refers to the conventional MLST approach employing six loci to type *C. glabrata* and PLOI refers to the approach proposed in this study. The resolution of each approach and locus is evaluated by three factors, namely precision, recall, and F1. The higher the overall score, the more resolutive is the approach/locus.

| Loci	Approach	Precision	Recall	F1
FKS1	MLST	0.96	0.87	0.88
LEU2	MLST	0.87	0.75	0.74
NMT1	MLST	0.93	0.93	0.93
TRP1	MLST	0.96	0.81	0.83
UGP1	MLST	0.79	0.85	0.77
URA3	MLST	0.92	0.78	0.79
A02255	PLOI	0.95	0.83	0.85
DUF1	PLOI	0.88	0.87	0.84
G00715	PLOI	0.83	0.91	0.86
G00825	PLOI	0.99	1.0	0.99
G03839	PLOI	0.92	0.82	0.82
G06281	PLOI	0.92	0.81	0.82
H09053	PLOI	0.92	0.81	0.83
HKR1	PLOI	0.97	0.90	0.91
PIR1	PLOI	0.90	0.86	0.85
PIR2	PLOI	0.94	0.88	0.90
SLG1	PLOI	0.99	1.0	0.99
SSR1	PLOI	0.96	0.95	0.95
USA1	PLOI	0.90	0.93	0.90

PLOI: Polymorphic loci of interest.

very different position in the tree can cause a marked increase in the RF metric as it will affect many partitions.

Clade comparison

We used ETE v. 3 to assess the monophyly of sequences from the same ST. This would indicate that the sequences used to reconstruct the tree have the capacity to correctly classify strains into the same clades as the MLST genes. In order to quantify the consistency between clades we calculated the precision, recall and F1 values of each ST in the following way: for each node in the tree, we established to which ST most of the sequences belong. Considering all OTUs (strains) contained within this partition, we considered as true positives (TP) the strains that belonged to the ST, and false positives (FP) those belonging to alternative STs, how many strains from the same ST appeared outside that partition, false negatives (FN) and how many leaves from the rest of the tree were from a different ST, true negatives (TN). For each node we calculated the precision, recall and F1 for the chosen ST. Then, for each ST we selected the node that offered the best F1. So for a ST that was found completely monophyletic we would obtain a F1 of 1.0. For each tree, we calculated the average precision, recall and F1 of all the ST groups.
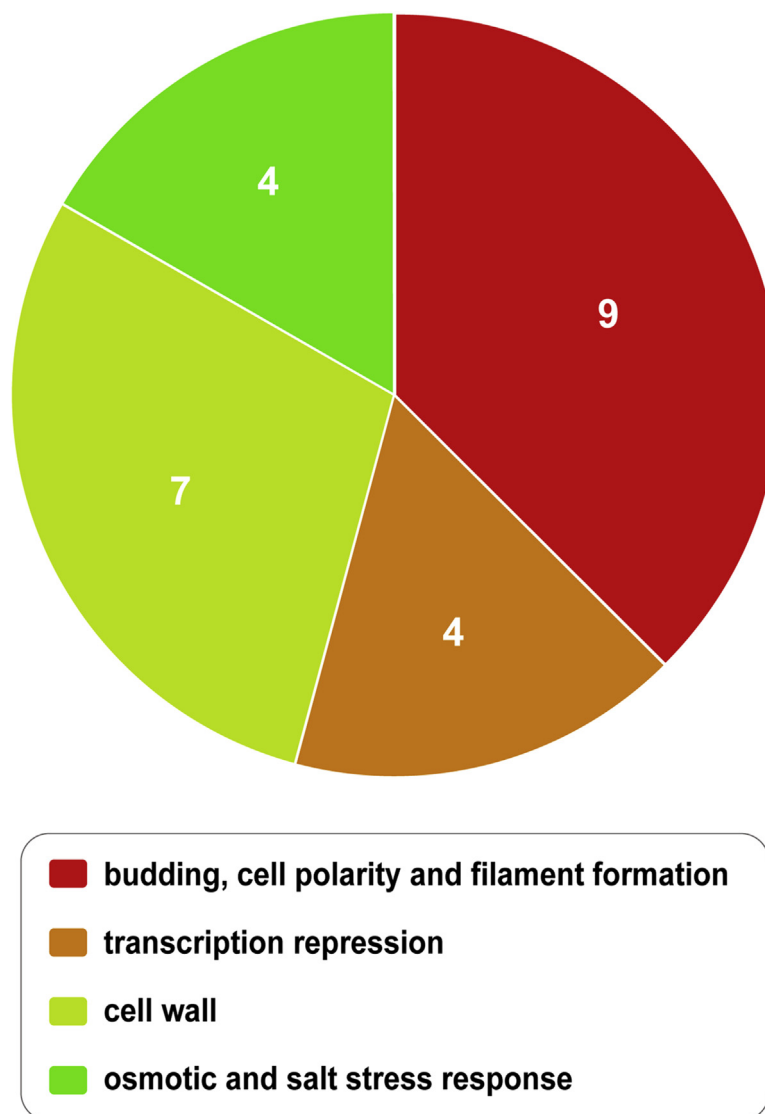
Fig. 3. The gene ontology enrichment to select the polymorphic loci (PL) of interest among a pool of candidate loci. Eleven loci involved in cellular integrity and stress response pathways and two loci lacking orthologs in *Saccharomyces cerevisiae* were selected for further analysis.
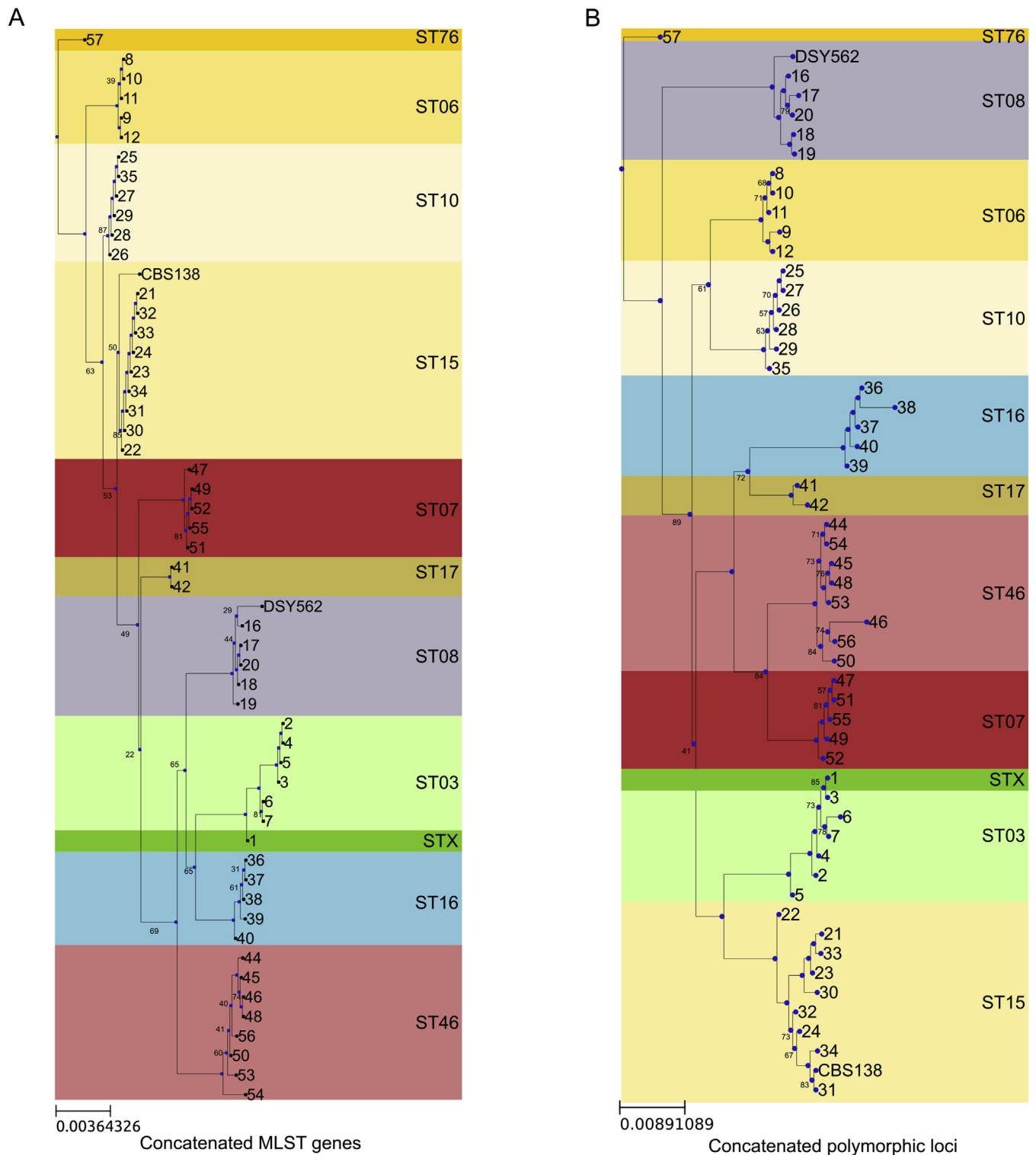
RESULTS

Genome variation among the isolates

The workflow of this study is shown in Fig. 1. Seven clinical isolates belonging to ST10 (28, 29, 35), 15 (30 and 33), and 16 (38 and 40) (Table 1), were processed for WGS by long-read (PacBio) and short-read (Illumina) methods. Their genomes were then assembled and compared to each other and to the reference strain CBS138/ATCC2001 (Xu *et al.* 2021). Consistent with expectations, this analysis showed that 387 to 1 063 SNPs separated strains of the same ST, whereas strains of different STs were 57 476 to 75 811 SNPs apart.

We also analysed the genomes for large-scale chromosomal variations known to frequently characterize *C. glabrata* strains (Carreté *et al.* 2018) (Fig. 2). Figure 2 shows the comparison between the seven newly sequenced genomes of *C. glabrata* and the CBS138 reference genome. Inversions, in

red, were not very common. The three main inversions observed were a small inversion in chromosome C present in four of the seven strains (ATCC90030 (#35), DPK305 (#28), DPL245 (#38) and CAS08-0027 (#30)), a large (> 600 Kb) inversion in chromosome L in DPL245 (#38), and a smaller inversion in chromosome L in CAS08-0016 (#40) just adjacent to previous one. None of the inversions were specific to a given ST. For instance, DPL245 (#38) and CAS08-0016 (#40) belong to the same ST and they both have an inversion in chromosome L, but these inversions do not affect the same region. The inversion in chromosome C is shared by two isolates of clade ST10 (ATCC90030 (#35) and DPK305 (#28)), but not present in the third one (CAS08-0425 (#29)). However, this inversion is also present in DPK762 (#33) (ST15) but not in the other ST15 strains (CAS08-0027 (#30) and the reference strain CBS138. Translocations are more common, though they predominantly affect telomeric regions and therefore could be the result of either miss-assemblies or miss-

Fig. 4. A. Tree resulting from the concatenation of six traditional MLST genes. Colours represent the ST group each strain belongs to. Bootstraps below 90 % are shown on the tree. **B.** Tree resulting from the concatenation of 13 hypervariable regions.

alignments. Still, some of the translocations are consistent across isolates and had already previously been described (Carreté *et al.* 2018). For instance, in four of the seven strains we see a translocation from chromosome L to chromosome D. This translocation is found in two of the three isolates of ST10 (ATCC90030 (35) and DPK305 (28)) and in the two strains of ST16 (DPL245 (38) and CAS08-0016 (40)). A second translocation moved a piece of chromosome D to chromosome L,

affecting two of the three strains of ST10 (ATCC90030 (35) and CAS08-0425 (29)). Three additional translocations affected DPL245 (38): pieces of chromosome D and chromosome L moved to chromosome I and a large part of chromosome I was found attached to chromosome L. Finally, pieces of chromosomes I and J were interchanged in the genome of CAS08-0027 (30). This translocation was not observed previously.

Table 5. Summary statistics for each group of trees

Statistics	Concatenated tree of MLST	Concatenated tree of PLOIs	1 gene	2 genes	3 genes	4 genes	5 genes	6 genes
Average Precision	-	-	0.93	0.97	0.98	0.98	0.98	0.98
Average Recall	-	-	0.89	0.94	0.97	0.98	0.99	0.995
Average F1	-	-	0.89	0.95	0.97	0.98	0.98	0.99
Maximum F1	1.0	0.99	0.99	0.99	0.99	0.99	0.99	0.99

PLOI: Polymorphic loci of interest.

Although changes in genome structure were not consistent with ST assignments, ST16 is the one most distantly related to the reference (CBS 138), both in terms of chromosome structure and DNA sequence (Fig. 2).

HPL selection and GEO

To identify discriminative HPL in *C. glabrata* that may be resolutive for ST, we aligned individual chromosomes from the seven newly assembled genomes with those from reference strain CBS138 and strain DSY562, for which high quality WGS is available (Vale-Silva *et al.* 2017, Xu *et al.* 2021). Highly polymorphic loci (HPL) were defined based on the presence of indels that were different between strains of different STs. To avoid overlap with previously published sets of loci, HPL associated with satellite regions, megasatellites, minisatellites, and microsatellites, were excluded (Thierry *et al.* 2008). In total 33 HPL were identified (Table 3), which were subjected to GO analysis using FungiFun (Priebe *et al.* 2015). Since the functions of most of the genes in *C. glabrata* are not characterized, their orthologs in *Saccharomyces cerevisiae* (https://www.yeastgenome.org) were used for GO analysis. These loci were found to be significantly enriched for stress response pathways, particularly those responding to cell surface (cell wall and plasma membrane) stress (Fig. 3), with 14 out of 33 loci containing genes involved in these processes. Our subsequent analyses focused on this subset of loci, with the exception of *UBI4*, which showed variation even among strains of the same ST and was therefore omitted, leaving 13 loci (Table 3).

Comparison of concatenated original MLST and HPL trees

To identify the most resolutive HPL, we sequenced the 13 HPL (Table 3) as well as the six loci used in the traditional MLST scheme in 53 additional *C. glabrata* clinical isolates belonging to 13 STs (Table 1). We built a tree based on the concatenation of the six traditional MLST genes and mapped ST information on it in different colors (Fig. 4A). The same was done with the 13 HPL (Fig. 4B). The trees were rooted at strain 57 as it is the only member of ST76. The two trees were very different in terms of the Robinson and Foulds calculation (RF), which is 0.72, meaning that 72 % of the nodes defined in the tree were different. These differences could be due to either the re-arrangements within STs, re-arrangements among STs, or strains moving between STs.

In order to compare the performance of the two means of generating phylogenetic trees (HPL vs traditional MLST loci), we computed the precision, recall and F1 for each ST and then calculated the average precision, recall and F1 for the whole

tree. The MLST concatenated tree, which can serve as baseline, showed a precision of 1.0, a recall of 1.0 and a F1 of 1.0, whereas the concatenated of the HPL had a slightly lower precision 0.99, a recall of 0.1.0 and a F1 of 0.99. While the tree based on MLST data recovered all ST perfectly, the tree based on HPL only failed in retrieving ST03 as a monophyletic clade due to the presence of STX.

Comparison of single gene trees

We repeated the same comparison with trees built for each single gene in the analysis. As seen in Table 4, out of the six MLST genes, *NMT1* was best able, on its own, to capture the variability of ST, though it did not perform as well as the concatenated assembly. Interestingly, two HPL were able to capture ST information better than *NMT1*: G00825 and *SLG1*. As seen in Fig. 5, *NMT1* was unable to distinguish between ST10 and ST15, which is not surprising because the

Table 6. Best combinations of two polymorphic loci.

Polymorphic loci combination	Alignment length	Precision
A02255;SLG1	1 549	0.99
DUF1;G00825	2 120	0.99
DUF1;SLG1	1 573	0.99
G00825;G03839	2 280	0.99
G00825;G06281	2 229	0.99
G00825;HKR1	2 874	0.99
G00825;SLG1	3 165	0.99
G00825;SRR1	2 519	0.99
G06281;SRR1	1 036	0.99
H09053;HKR1	1 252	0.99
H09053;SLG1	1 543	0.99
HKR1;PIR2	2 035	0.99
HKR1;SLG1	2 327	0.99
HKR1;SRR1	1 681	0.99
HKR1;USA1	1 558	0.99
PIR2;SLG1	2 326	0.99
PIR2;SRR1	1 680	0.99
PIR2;USA1	1 557	0.99
SLG1;SRR1	1 972	0.99
SLG1;USA1	1 849	0.99
SRR1;USA1	1 203	0.99
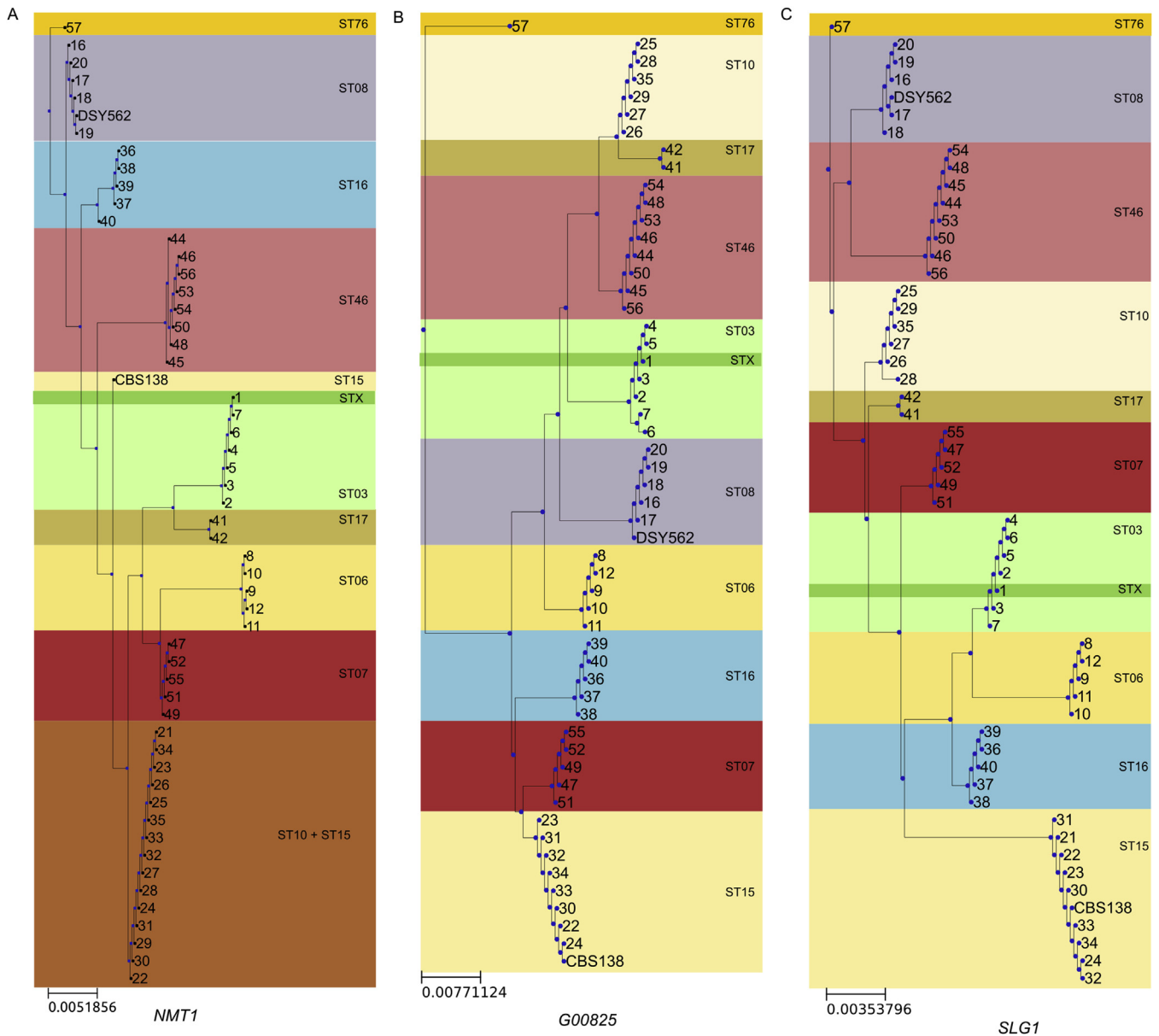
Fig. 5. Single gene trees belonging to **A.** *NMT1*, **B.** *G00825* and **C.** *SLG1*. Clades are colored according to the ST group. In *NMT1* ST10 and ST15 are colored in the same color as they are identical in all strains.

distinction between these two ST is based on the classification of *LEU2* and *URA3*. It is also unable to separate STX from ST03, whose separation is again determined by a different gene (*TRP1*). In contrast, the two best HPL were able to separate ST10 from ST15 but could not separate STX from ST03 (Fig. 5).

Comparison of concatenated gene trees using combinations of loci

STs are currently assigned based on the allelic information provided by six genes. As single genes are not able to completely recover all ST groups as monophyletic clades, we tried to find a combination of six or fewer genes that could perform better than the concatenated MLST tree. To do that, we generated concatenated alignments of combinations of 2, 3, 4, 5 and 6 HPL and checked them for the distribution of ST. We then calculated the

average precision, recall and F1 (Table 5). We found that none of the combinations performed as the concatenated MLST tree. However, 21 different combinations of two HPL genes were able to recover the same ST distribution as found by the concatenation of HPL, showing that few genes have as much resolutive power as the 13 selected HPL (Table 6 and Supplementary Table 1).

Finally, we tested whether combining MLST genes with HPL would produce better results. Two combinations of *TRP1* with a single HPL (either SLG1 or G00825) resulted in a tree which was as good as the concatenated tree based on the six MLST loci (Figs 5 and 6).

CONCLUSIONS

Understanding the genetic diversity of *C. glabrata* isolates has broad clinical and biological implications ranging from aiding effective implementation of infection control strategies in
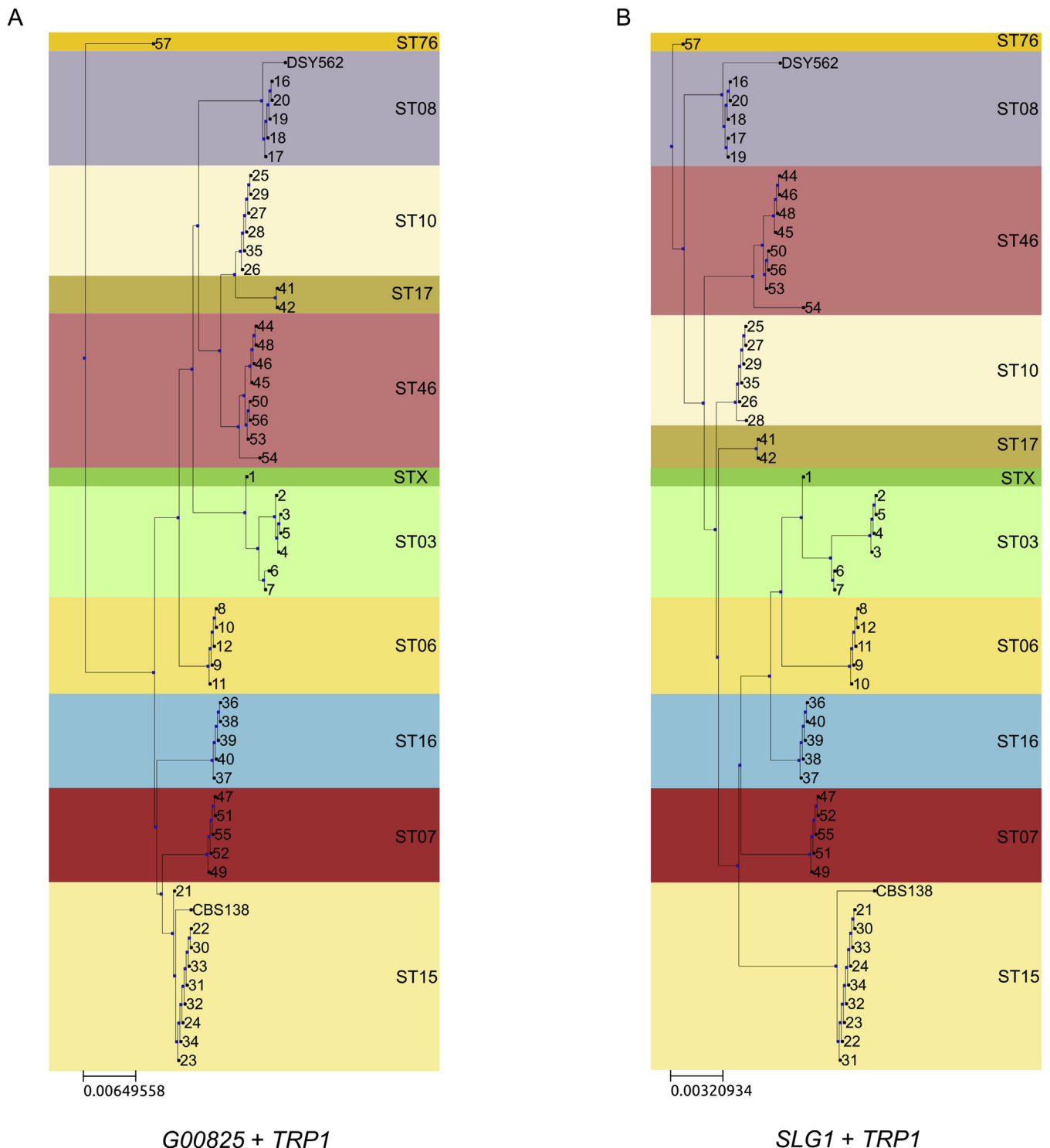
Fig. 6. Trees based on the concatenation of two genes. **A.** *G00825 + TRP1*. **B.** *SLG1 + TRP1*.

hospitals to understanding within-host microevolution, which can help answer key questions regarding host-pathogen interaction and the development of antifungal resistance. In this study we used WGS and comparative genomic analyses to identify a new MLST scheme based not only on SNPs but also indels, and, using only two loci, offers the same resolution as that provided by the widely used six-locus MLST scheme. Using 53 clinical *C. glabrata* isolates originating from various geographical regions and belonging to different STs, we showed that the two-locus scheme was in 100 % agreement with the traditional MLST

approach. Also, we note that except for isolate CAS08-0293 for which the ST could not be distinguished with HPL, the ST of the rest of the isolates were successfully determined when testing only *SLG1* or G00825. In summary, the newly described MLST scheme can be used as a reliable approach for high throughput typing purposes in clinical settings and large-scale studies aiming to understand the genetic diversity *of C. glabrata* globally. Additionally, the high-quality whole genomes of seven clinical strains reported in this study can serve as references for future short read based WGS analyses of *C. glabrata*, helping the field

develop new diagnostic tools and address fundamental biological questions.

DATA AVAILABILITY

The project has been deposited in GenBank under the Bioproject number PRJNA718446. The raw read data are deposited under accession number SRR8146337. Read data and genome assemblies can be found under SRA codes SRR14180810 to SRR14180816 for the Illumina reads and codes SRR14163270 to SRR14163276 for PacBio reads. MLST and PL sequences were deposited in GenBank under codes MW970414 to MW971421. Accession numbers associated with the isolates whole-genome sequenced were as follows, JAGTUA000000000 (CAS08-0425), JAGTTZ000000000 (CAS80027), JAGTT Y000000000 (DPK762), JAGTTX000000000 (ATCC 90030), JAGTTW000000000 (DPL245), JAGTTV000000000 (CAS08-0016), JAGTTU000000000 (DPK 305).

ACKNOWLEDGEMENTS

APPENDIX A. SUPPLEMENTARY DATA

Supplementary data to this article can be found online at https://doi.org/10.1016/j.simyco.2021.100133.

REFERENCES

Arastehfar A, Yazdanpanah S, Bakhtiari M, *et al*. (2020a). Epidemiology of candidemia in Shiraz, southern Iran: A prospective multicenter study (2016-2018). *Medical Mycology* **59**: 422–430.

Arastehfar A, Lass-flörl C, Garcia-rubio R, *et al*. (2020b). The quiet and underappreciated rise of drug-resistant invasive fungal pathogens. *Journal of Fungi* **6**: 138.

Arastehfar A, Daneshnia F, Salehi MR, *et al*. (2020c). Low level of antifungal resistance of *Candida glabrata* blood isolates in Turkey: Fluconazole minimum inhibitory concentration and FKS mutations can predict therapeutic failure. *Mycoses* **63**: 911–920.

Arastehfar A, Daneshnia F, Najafzadeh J, *et al*. (2020d). Evaluation of molecular epidemiology, clinical characteristics, antifungal susceptibility profiles, and molecular mechanisms of antifungal resistance of Iranian *Candida parapsilosis* species complex blood isolates. *Frontiers in Cellular and Infection Microbiology* **10**: 206.

Arastehfar A, Daneshnia F, Zomorodian K, *et al*. (2019). Low level of antifungal resistance in Iranian isolates of *Candida glabrata* recovered from Blood samples in a multicenter study from 2015 to 2018 and potential prognostic values of genotyping and sequencing of PDR1. *Antimicrobial Agents Chemotherapy* **63**: e02503–e02518.

Astvad KMT, Johansen HK, Røder BL, *et al*. (2018). Update from a 12-year nationwide fungemia surveillance: increasing intrinsic and acquired resistance causes concern. *Journal of Clinical Microbiology* **56**: e01564–e01617.

Biswas C, Marcelino VR, Van Hal S, *et al*. (2018). Whole genome sequencing of australian *Candida glabrata* isolates reveals genetic diversity and novel sequence types. *Frontiers in Microbiology* **9**: 2946.

Boetzer M, Pirovano W (2014). SSPACE-LongRead: scaffolding bacterial draft genomes using long read sequence information. *BMC Bioinformatics* **15**: 211.

Bordallo-Cardona MÁ, Agnelli C, Gómez-Nuñez A, *et al*. (2019). *MSH2* gene point mutations are not antifungal resistance markers in *Candida glabrata*. *Antimicrobial Agents and Chemotherapy* **63**: e01876–e01918.

Brown GD, Denning DW, Gow NAR, *et al*. (2012). Hidden killers: Human fungal infections. *Science Translational Medicine* **4**: 165rv13.

Byrne KP, Wolfe KH (2005). The yeast gene order browser: combining curated homology and syntenic context reveals gene fate in polyploid species. *Genome Research* **15**: 1456–1461.

Byun SA, Won EJ, Kim MN, *et al*. (2018). Multilocus sequence typing (MLST) genotypes of *Candida glabrata* bloodstream isolates in Korea: association with antifungal resistance, mutations in mismatch repair gene (Msh2), and clinical outcomes. *Frontiers in Microbiology* **9**: 1523.

Carreté L, Ksiezopolska E, Gómez-Molero E, *et al*. (2019). Genome comparisons of *Candida glabrata* serial clinical isolates reveal patterns of genetic variation in infecting clonal populations. *Frontiers in Microbiology* **10**: 112.

Carreté L, Ksiezopolska E, Pegueroles C, *et al*. (2018). Patterns of genomic variation in the opportunistic pathogen *Candida glabrata* suggest the existence of mating and a secondary association with humans. *Current Biology* **28**: 15–27.e7.

Chakrabarti A, Sood P, Rudramurthy SM, *et al*. (2015). Incidence, characteristics and outcome of ICU-acquired candidemia in India. *Intensive Care Medicine* **41**: 285–295.

Chapman B, Slavin M, Marriott D, *et al*. (2017). Changing epidemiology of candidaemia in Australia. *Journal Antimicrobial Chemotherapy* **72**: 1103–1108.

Clinical and Laboratory Standards Institute (2017). *Performance standards for antifungal susceptibility testing of yeasts*. Approved standard M60. CLSI, Wayne, PA.

DePristo MA, Banks E, Poplin R, *et al*. (2011). A framework for variation discovery and genotyping using next-generation DNA sequencing data. *Nature Genetics* **43**: 491–498.

Dodgson AR, Pujol C, Denning DW, *et al*. (2003). Multilocus sequence typing of *Candida glabrata* reveals geographically enriched clades. *Journal of Clinical Microbiology* **41**: 5709–5717.

English AC, Richards S, Han Y, *et al*. (2012). Mind the gap: upgrading genomes with Pacific Biosciences RS long-read sequencing technology. *PLoS One* **7**: e47768.

Fuller J, Dingle TC, Bull A, *et al*. (2019). Species distribution and antifungal susceptibility of invasive Candida isolates from Canadian hospitals: results of the CANWARD 2011-16 study. *Journal of Antimicrobial Chemotherapy* **74**: iv48–iv54.

Gabaldón T (2019). Recent trends in molecular diagnostics of yeast infections: from PCR to NGS. *FEMS Microbiology Reviews* **43**: 517–547.

Gabaldón T, Fairhead C (2019). Genomes shed light on the secret life of *Candida glabrata*: not so asexual, not so commensal. *Current Genetics* **65**: 93–98.

Gabaldón T, Gómez-Molero E, Bader O (2020). Molecular typing of *Candida glabrata*. *Mycopathologia* **185**: 755–764.

Gremme G, Brendel V, Sparks MES (2005). Engineering a software tool for gene structure prediction in higher organisms. *Information and Software Technology* **47**: 965–978.

Haas BJ, Salzberg SL, Zhu W, *et al*. (2008). Automated eukaryotic gene structure annotation using EVidenceModeler and the program to assemble spliced alignments. *Genome Biology* **9**: R7.

Healey KR, Perlin DS (2018). Fungal resistance to cchinocandins and the MDR phenomenon in *Candida glabrata*. *Journal of Fungi* **4**: 105.

Holt C, Yandell M (2011). MAKER2: an annotation pipeline and genome-database management tool for second-generation genome projects. *BMC Bioinformatics* **12**: 491.

Hou X, Xiao M, Chen SCA, *et al*. (2017). Molecular epidemiology and antifungal susceptibility of *Candida glabrata* in China (August 2009 to July 2014): a multi-center study. *Frontiers in Microbiology* **8**: 880.

Hou X, Xiao M, Wang H, *et al*. (2018). Profiling of *PDR1* and *MSH2* in *Candida glabrata* bloodstream isolates from a multicenter study in China. *Antimicrobial Agents Chemotherapy* **62**: e00153–e00218.

Huerta-Cepas J, Dopazo J, Gabaldón T (2010). ETE: a python environment for tree exploration. *BMC Bioinformatics* **11**: 24.

Katiyar S, Edlind T (2021). New locus for *Candida glabrata* sequence-based strain typing provides evidence for nosocomial transmission. *Journal of Clinical Microbiology* **59**: e02933–e03020.

Katiyar S, Shiffrin E, Shelton C, *et al.* (2016). Evaluation of polymorphic locus sequence typing for *Candida glabrata* epidemiology. *Journal of Clinical Microbiology* **54**: 1042–1050.

Khalifa HO, Arai T, Majima H, *et al.* (2020). Genetic basis of azole and echinocandin resistance in clinical *Candida glabrata* in Japan. *Antimicrobial Agents and Chemotherapy* **64**: e00783–e00820.

Kord M, Salehi M, Khodavaisy S, *et al.* (2020). Epidemiology of yeast species causing bloodstream infection in Tehran, Iran (2015 – 2017); superiority of 21-plex PCR over the Vitek 2 system for yeast identification. *Journal of Medical Microbiology* **69**: 712–720.

Koren S, Walenz BP, Berlin K, *et al.* (2017). Canu: scalable and accurate long-read assembly via adaptive k-mer weighting and repeat separation. *Genome Research* **27**: 722–736.

Ksiezopolska E, Gabaldón T (2018). Evolutionary emergence of drug resistance in *Candida* opportunistic pathogens. *Genes* **9**: 461.

Lamoth F, Lockhart SR, Berkow EL, *et al.* (2018). Changes in the epidemiological landscape of invasive candidiasis. *The Journal of Antimicrobial Chemotherapy* **73**: i4–i13.

Li H, Durbin R (2009). Fast and accurate short read alignment with Burrows-Wheeler transform. *Bioinformatics* **25**: 1754–1760.

Lin CY, Chen YC, Lo HJ, *et al.* (2007). Assessment of *Candida glabrata* strain relatedness by pulsed-field gel electrophoresis and multilocus sequence typing. *Journal of Clinical Microbiology* **45**: 2452–2459.

Lott TJ, Frade JP, Lockhart SR (2010). Multilocus sequence type analysis reveals both clonality and recombination in populations of *Candida glabrata* bloodstream isolates from U.S. surveillance studies. *Eukaryotic Cell* **9**: 619–625.

Lott TJ, Frade JP, Lyon GM, *et al.* (2012). Bloodstream and non-invasive isolates of *Candida glabrata* have similar population structures and fluconazole susceptibilities. *Medical Mycology* **50**: 136–142.

Megri Y, Arastehfar A, Boekhout T, *et al.* (2020). *Candida tropicalis* is the most prevalent yeast species causing candidemia in Algeria: the urgent need for antifungal stewardship and infection control measures. *Antimicrobial Resistance and Infection Control* **9**: 50.

Otto TD, Dillon GP, Degrave WS, *et al.* (2011). RATT: Rapid annotation transfer tool. *Nucleic Acids Research* **39**: e57.

Pappas PG, Kauffman CA, Andes DR, *et al.* (2016). Clinical practice guideline for the management of candidiasis : 2016 update by the Infectious Diseases Society of America. *Clinical Infectious Diseases* **62**: 1–50.

Pfaller MA, Diekema DJ (2012). Progress in antifungal susceptibility testing of *Candida* spp. by use of Clinical and Laboratory Standards Institute broth microdilution methods, 2010 to 2012. *Journal of Clinical Microbiology* **50**: 2846–2856.

Pfaller MA, Diekema DJ, Turnidge JD, *et al.* (2019). Twenty years of the SENTRY antifungal surveillance program: results for *Candida* species from 1997-2016. *Open Forum Infectious Diseases* **6**: S79–S94.

Pfaller MA, Messer SA, Hollis RJ, *et al.* (2009). Variation in susceptibility of bloodstream isolates of *Candida glabrata* to fluconazole according to patient age and geographic location in the United States in 2001 to 2007. *Journal of Clinical Microbiology* **47**: 3185–3190.

Priebe S, Kreisel C, Horn F, *et al.* (2015). FungiFun2: a comprehensive online resource for systematic analysis of gene lists from fungal species. *Bioinformatics* **31**: 445–446.

Proux-Wéra E, Armisén D, Byrne KP, *et al.* (2012). A pipeline for automated annotation of yeast genome sequences by a conserved-synteny approach. *BMC Bioinformatics* **13**: 237.

Romo JA, Kumamoto CA (2020). On commensalism of *Candida*. *Journal of Fungi* **6**: 16.

Slater GSC, Birney E (2005). Automated generation of heuristics for biological sequence comparison. *BMC Bioinformatics* **6**: 31.

Song Y, Chen X, Yan Y, *et al.* (2020). Prevalence and antifungal susceptibility of pathogenic yeasts in China: a 10-year retrospective study in a teaching hospital. *Frontiers in Microbiology* **11**: 1401.

Stavrou AA, Lackner M, Lass-Flörl C, Boekhout T (2019). The changing spectrum of *Saccharomycotina* yeasts causing candidemia: phylogeny mirrors antifungal susceptibility patterns for azole drugs and amphotericin B. *FEMS Yeast Research* **19**: 4.

Taj-Aldeen SJ, Kolecka A, Boesten R, *et al.* (2014). Epidemiology of candidemia in Qatar, the Middle East: performance of MALDI-TOF MS for the identification of *Candida* species, species distribution, outcome, and susceptibility pattern. *Infection* **42**: 393–404.

Thierry A, Bouchier C, Dujon B, *et al.* (2008). Megasatellites: a peculiar class of giant minisatellites in genes involved in cell adhesion and pathogenicity in *Candida glabrata*. *Nucleic Acids Research* **36**: 5970–5982.

Tsay SV, Mu Y, Williams S, *et al.* (2020). Burden of candidemia in the United States, 2017. *Clinical Infectious Diseases* **71**: e449–e453.

Vale-Silva L, Beaudoing E, Tran VDT, *et al.* (2017). Comparative genomics of two sequential *Candida glabrata* clinical isolates. *G3* **7**: 2413–2426.

Won EJ, Choi MJ, Kim MN, *et al.* (2021). Fluconazole-resistant *Candida glabrata* bloodstream isolates, South Korea, 2008-2018. *Emerging Infectious Diseases* **27**: 779–788.

Xu Z, Green B, Benoit N, *et al.* (2021). Cell wall protein variation, break induced replication, and subtelomere dynamics in *Candida glabrata*. *Molecular Microbiology*. https://doi.org/10.1111/mmi.14707. Online ahead of print.